



UNIVERSITÀ
DEGLI STUDI
FIRENZE

FLORE

Repository istituzionale dell'Università degli Studi di Firenze

Combining in-cell NMR and X-ray fluorescence microscopy to reveal the intracellular maturation states of human superoxide dismutase 1.

Questa è la Versione finale referata (Post print/Accepted manuscript) della seguente pubblicazione:

Original Citation:

Combining in-cell NMR and X-ray fluorescence microscopy to reveal the intracellular maturation states of human superoxide dismutase 1 / Enrico Luchinat; Alessandra Gianoncelli; Tommaso Mello; Andrea Galli; Lucia Banci. - In: CHEMICAL COMMUNICATIONS. - ISSN 1359-7345. - STAMPA. - 51:(2015), pp. 584-587. [10.1039/c4cc08129c]

Availability:

The webpage <https://hdl.handle.net/2158/960645> of the repository was last updated on 2024-02-08T15:52:35Z

Published version:

DOI: 10.1039/c4cc08129c

Terms of use:

Open Access

La pubblicazione è resa disponibile sotto le norme e i termini della licenza di deposito, secondo quanto stabilito dalla Policy per l'accesso aperto dell'Università degli Studi di Firenze (<https://www.sba.unifi.it/upload/policy-oa-2016-1.pdf>)

Publisher copyright claim:

Conformità alle politiche dell'editore / Compliance to publisher's policies

Questa versione della pubblicazione è conforme a quanto richiesto dalle politiche dell'editore in materia di copyright.

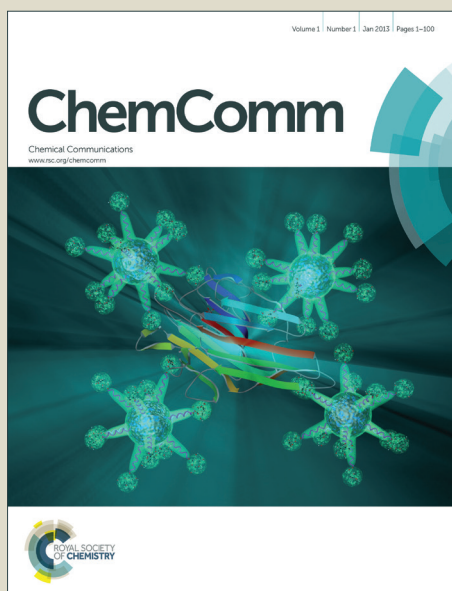
This version of the publication conforms to the publisher's copyright policies.

La data sopra indicata si riferisce all'ultimo aggiornamento della scheda del Repository FloRe - The above-mentioned date refers to the last update of the record in the Institutional Repository FloRe

(Article begins on next page)

ChemComm

Accepted Manuscript



This is an *Accepted Manuscript*, which has been through the Royal Society of Chemistry peer review process and has been accepted for publication.

Accepted Manuscripts are published online shortly after acceptance, before technical editing, formatting and proof reading. Using this free service, authors can make their results available to the community, in citable form, before we publish the edited article. We will replace this *Accepted Manuscript* with the edited and formatted *Advance Article* as soon as it is available.

You can find more information about *Accepted Manuscripts* in the [Information for Authors](#).

Please note that technical editing may introduce minor changes to the text and/or graphics, which may alter content. The journal's standard [Terms & Conditions](#) and the [Ethical guidelines](#) still apply. In no event shall the Royal Society of Chemistry be held responsible for any errors or omissions in this *Accepted Manuscript* or any consequences arising from the use of any information it contains.

COMMUNICATION

Combining in-cell NMR and X-ray fluorescence microscopy to reveal intracellular maturation states of human superoxide dismutase 1

Cite this: DOI: 10.1039/x0xx00000x

E. Luchinat,^{a,b} A. Gianoncelli,^c T. Mello,^b A. Galli^b and L. Banci^{*a,d}

Received 00th January 2012,

Accepted 00th January 2012

DOI: 10.1039/x0xx00000x

www.rsc.org/

An integrated approach which combines in-cell NMR spectroscopy with optical and X-ray fluorescence microscopy was developed to describe the intracellular maturation state of human Cu,Zn-SOD1. Microscopy data show a correlation between the intracellular levels of SOD1 and the content of zinc, corresponding to zinc binding to SOD1 observed by in-cell NMR.

Detailed understanding of cellular processes requires knowledge of the macromolecules involved, on their localization within the cell, and their atomic resolution description. Classically, these data are collected separately with different techniques, on very different types of samples for each experiment. Intact – ideally live – cells are used for protein localization; purified proteins, crystallized or in solution, for structure characterization; fixed/frozen cells, whole or sectioned, for electron and X-ray microscopy. Although this reductionist approach is extremely powerful – much of today's knowledge is built on these foundations – new approaches are required to integrate and correlate such different techniques, in order to allow intracellular description – at all the resolutions – of the macromolecules of interest. Nuclear magnetic resonance (NMR) spectroscopy has already been extended to live-cell studies.¹ In-cell NMR allows structural and functional characterization of proteins inside living mammalian cells, at atomic resolution.^{2,3} However, due to the intrinsically low sensitivity, NMR data are obtained on samples of millions of cells, and lack spatial resolution.

In this work, we sought to establish a new approach for combining and correlating atomic-level structural information of metalloproteins obtained in live human cells with their intracellular distribution, their levels of expression and their metal cofactors. For this purpose, we combined in-cell NMR with synchrotron radiation X-ray fluorescence (XRF) microscopy, which measures the elemental distribution within

single cells, and is ideally applied to trace elements, such as transition metals.^{4,5} Optical fluorescence microscopy was also used on the same cells to correlate the intracellular distribution of metal cofactors with the intracellular distribution – and expression levels – of the proteins of interest.

As a model system, we focused on the maturation steps of human copper-zinc superoxide dismutase 1 (Cu,Zn-SOD1). SOD1 is a 32 kDa homodimeric protein involved in the cellular defence against oxidative stress, mainly localized in the cytosol.⁶ To reach the mature state, SOD1 needs to bind one structural zinc ion per monomer, to dimerize, and to bind a catalytic copper ion per monomer. Additionally, an intramolecular disulfide bond has to form between two conserved cysteines. The copper binding and cysteine oxidation steps require interaction with the copper chaperone for SOD1 (CCS).⁷ It has been previously shown that the folding, metallation and oxidation states of SOD1 at different maturation steps could be identified and characterized in the human cytoplasm by in-cell NMR.³

Here, cells overexpressing SOD1 and/or CCS with different amounts of zinc and copper ions were analyzed by both optical and XRF microscopy, and the resulting data were correlated with the information obtained by in-cell NMR. A relationship was established between the intracellular levels of SOD1 and the zinc content in each cell, as intracellular SOD1 spontaneously binds the zinc available in excess. Conversely, copper treatment resulted in increased copper content in all treated cells, and no clear correlation could be established between copper levels and either SOD1 or CCS. The cell response to external copper involves other copper-binding molecules such as metallothioneins, which likely caused the observed increase in cellular copper content. The approach described here can potentially be extended to describe metalloprotein maturation events at subcellular resolution.

The intracellular distribution of overexpressed SOD1 and

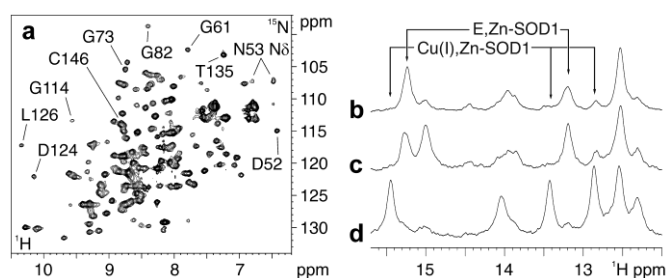


Fig. 1 (a) ^1H - ^{15}N correlation NMR spectrum acquired on human cells expressing uniformly ^{15}N -labeled SOD1 in zinc-supplemented medium. Residues sensitive to the metallation and redox states of SOD1 are indicated. Chemical shift comparison with *in vitro* NMR spectra of SOD1 in different metallation and redox states shows that cytoplasmic SOD1 is homodimeric with one zinc ion bound per monomer (see Fig. S2); (b-d) ^1H NMR spectra acquired on cells expressing (b) SOD1 in zinc-supplemented medium, (c) SOD1 and CCS in zinc-supplemented medium, (d) same as (c) after incubation with copper. The spectral region containing the HN resonances of SOD1 metal-bound histidine rings is shown. Histidine protons assigned to E,Zn-SOD1 and Cu(I),Zn-SOD1 species are indicated.

CCS was analyzed by immunofluorescence microscopy on fixed cells expressing different levels of each protein. Both proteins were uniformly distributed throughout the cytoplasm (Fig. S1) as previously reported.³ CCS appeared slightly more concentrated towards the cell membrane, consistently with the protein being undetectable by in-cell NMR,³ and with the recent hypothesis that it interacts with the plasma membrane to facilitate its metallochaperone function.⁸

NMR analysis of intracellular SOD1 expressed in cells treated with excess zinc showed that SOD1 stoichiometrically bound one Zn^{2+} per monomer, indicating that no specific chaperone is necessary for this maturation step, and no apo-SOD1 was detected (Fig. 1a and Fig. S2).³ It is therefore expected that the total intracellular zinc would increase at increasing levels of SOD1. Indeed, the elemental maps obtained by XRF microscopy on cells treated with zinc during expression of SOD1 showed that cells with higher levels of SOD1 had a higher content of zinc (Fig. 2a-d). To account for the different volume of each cell, the elemental maps of copper and zinc were normalized by the X-ray scattering intensity (Fig. S3), which is linearly dependent on the sample thickness along the z-axis (Fig. S4). SOD1 concentration was also obtained by normalizing the optical fluorescence intensity of each cell by the X-ray scattering, and taking a monomer concentration of 10 μM for cells expressing endogenous levels of SOD1.³ The concentration of zinc in the normalized elemental maps was homogeneous within the area of each cell, consistent with the diffuse, cytosolic distribution of SOD1. Zinc concentration (in arbitrary units) shows a roughly linear relationship with SOD1 concentration for each cell (Fig. 2e), indicating that the increase in zinc content is indeed due to SOD1 stoichiometrically binding zinc. Cells with the highest levels of SOD1 ($\sim 200 \mu\text{M}$) showed an increase in total zinc content higher than two-fold, compared to cells expressing the lowest SOD1 levels (around 50 μM , Fig. 2e). As SOD1 binds 1 Zn^{2+} per monomer, the residual cellular zinc concentration (i.e. zinc not bound to SOD1) was estimated by linear regression around 100 μM . This value is lower than the reported total zinc concentration in

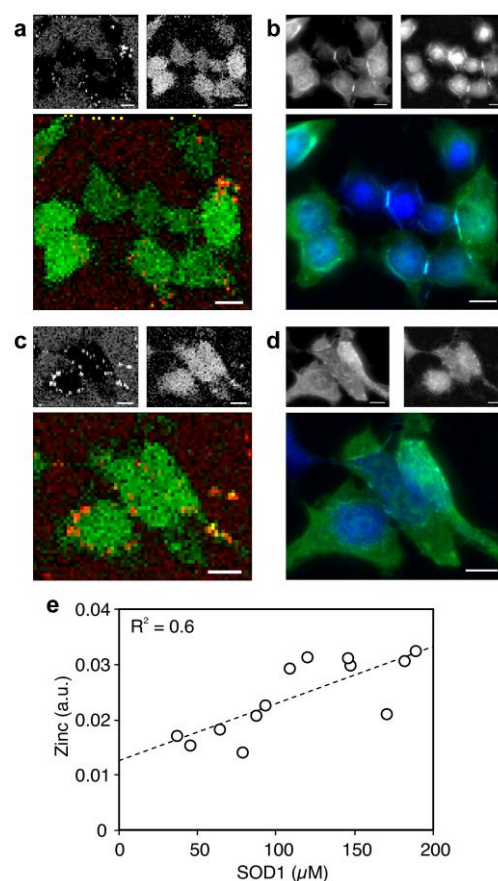


Fig. 2 (a,c) XRF microscopy images of cells overexpressing SOD1 at different levels, normalized by the X-ray scattering intensity, showing the intracellular distribution of copper (red channel, top left subpanel) and zinc (green channel, top right subpanel; composite, bottom subpanel); (b,d) optical microscopy images of the same cells, showing the expression levels and distribution of SOD1 (green channel, top left subpanel), and nuclear staining (blue channel, top right subpanel; composite, bottom subpanel). Scale bar = 10 μm . (e) zinc concentration (in arbitrary units) plotted against the estimated concentration of SOD1 (μM). Each dot corresponds to a single cell in panels a-d.

mammalian cells,⁹ possibly due to loosely bound zinc being lost during cell permeabilization.¹⁰ The average zinc concentration in untreated cells, measured by inductively coupled plasma-atomic emission spectroscopy (ICP-AES) on non-fixed cells grown in the same conditions, was $300 \pm 30 \mu\text{M}$ (s.d., $n=3$), confirming that some metal loss occurred during sample treatment. Cells overexpressing CCS together with SOD1 showed a similar behaviour: the zinc content only correlated with the intracellular concentration of SOD1, and was not influenced by increased CCS levels (Fig. 3a,b and Fig. 4a).

In copper-untreated cells, the amount and distribution of endogenous copper were not affected by increased levels of SOD1 and/or CCS. Most of copper retained a characteristic localization in the perinuclear region and close to the lamellipodia (Fig. 2a,c), which did not correlate with the homogeneous distribution of SOD1 and CCS (Fig. 2b,d). This localization pattern was observed before for copper, and likely arises from ATP7A protein trafficking between the Golgi network and the plasma membrane¹¹ and possibly from the mitochondrial copper pool.⁴ Consistently, when cytoplasmic

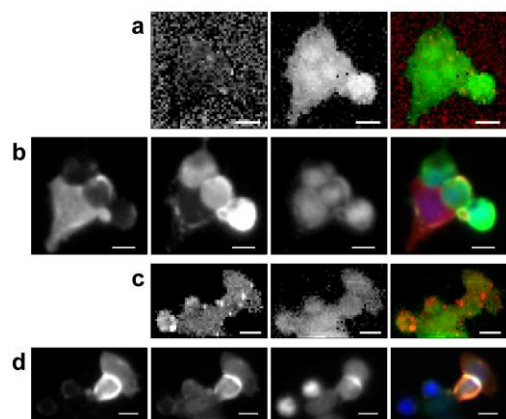


Fig. 3 (a,c) XRF microscopy images of cells co-expressing SOD1 and CCS at different levels, normalized by the X-ray scattering intensity, showing the intracellular distribution of zinc (green) and copper (red). From left to right: red channel, green channel, composite. (b,d) optical microscopy images of the same cells, showing the expression levels and distribution of SOD1 (green), CCS (red) and nuclear staining with DAPI (blue). From left to right: red channel, green channel, blue channel, composite. (a,b) cells not treated with external copper; (c,d) cells treated with copper. Scale bar = 10 μ m.

SOD1 is co-expressed with CCS but without copper addition, Cu,Zn-SOD1 is not formed at detectable levels (Fig. 1b).

In-cell NMR also showed that intracellular SOD1 did not bind copper spontaneously, even when the latter was supplemented in excess to the cells, with endogenous levels of CCS.³ Conversely, increased levels of CCS promoted copper delivery to SOD1 upon copper treatment, and fully mature Cu,Zn-SOD1 was formed (Fig. 1c). A marked increase in copper content (4-fold on average) was measured in copper-treated cells with respect to cells with basal levels of copper (Fig. 4b,d). The cellular copper content increase was observed in all cells, and did not correlate with the expression levels of either SOD1, CCS or both (Fig. 4d). ICP-AES analysis of total copper in non-fixed cells confirmed the data obtained by XRF, as untreated cells contained 40 ± 5 μ M copper (s.d., $n=3$), whereas copper-treated cells almost reached 1 mM copper. Notably, the surplus copper distributed uniformly in the cells, with seemingly no effect on the basal copper distribution, indicating that most of the newly imported copper diffusely localized in the cytosol (Fig. 3c,d). These data suggest that the observed increase in copper content is due to binding to other cellular components, such as metallothioneins, which act as buffers to regulate the concentration of available copper in the cytoplasm. Metallothionein gene expression is known to be regulated by oxidative stress and metal ions, and therefore increased metallothionein levels could explain the lack of correlation between copper content and SOD1/CCS levels.¹² Furthermore, in copper-treated cells the zinc content did not correlate with SOD1 levels (Fig. 4c), while a general increase (about 2-fold) in zinc content was observed compared to copper-untreated cells. Thus, copper treatment seemingly had an effect on cellular zinc content, which also could be due to increased metallothionein expression.

Conclusions

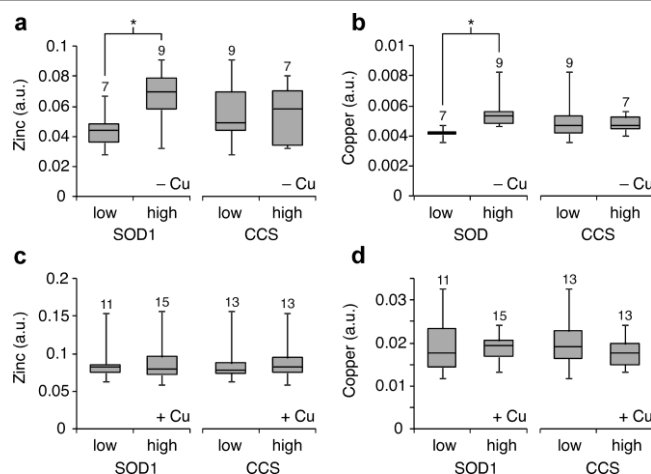


Fig. 4 Box and whisker plots showing the distribution of zinc (a,c) and copper (b,d) content in cells expressing different levels of SOD1 and CCS. Plots (a,b) were obtained from cells not treated with copper, (c,d) from copper-treated cells. Each plot is obtained from a set of single-cell averaged concentration values (see Fig. 2e); the number of samples is indicated on each box. * indicates significant differences (unpaired t-test, $p < 0.05$). Protein level is calculated relative to the lowest-expressing cells, measured from the optical fluorescence images (see Supplementary Methods). SOD1 concentration in (a,b): low < 30 μ M, high = 30-400 μ M; in (c,d): low < 50 μ M, high = 50-500 μ M. CCS relative overexpression in (a,b): low < 3 \times , high = 3-15 \times ; in (c,d): low < 10 \times , high = 10-70 \times .

The approach proposed in this work combines for the first time atomic-level information on protein metallation states by in-cell NMR, with protein localization by immunofluorescence microscopy and metal localization by XRF microscopy. All three techniques were applied on the same biological samples (although additional sample treatment was required for microscopy), thereby allowing easy correlation between the data. By using this approach, we identified SOD1 overexpression and zinc binding as the cause of intracellular zinc content increase, and we observed that the cellular response to copper treatment was masking the increase in copper due to actual metal delivery to SOD1.

Currently, the resolution is limited both by the sample preparation requirements, as air-drying the cells introduces artefacts due to refraction index mismatch, and by the resolution limit of the XRF instrument. XRF microscopy has recently seen much progress in terms of resolution and sensitivity, and is being applied to analyze biological specimen at increasing detail.¹³ On the other hand in-cell NMR, while usually applied to investigate cytosolic proteins, has recently been able to detect proteins inside subcellular compartments.¹⁴ As further progresses are to be expected in both fields, our combined approach has a broad applicability to investigate maturation of metalloproteins and protein-mediated metal transfer interactions at subcellular level.

This work was supported by the Instruct R&D Pilot Project “From single molecules to the cell: combining in cell NMR with light and X-ray microscopies” and by ESFRI Instruct Core Centre CERM – Italy. We thank Elettra-Sincrotrone Trieste for beamtime access; Prof. Roberto Udisti and Dr. Mirko Severi, University of Florence, for technical assistance on ICP-AES experiments; Dr. Damiano Cassese, CNR-IOM TASC

Laboratory Trieste, for AFM data; and Dr. Burkhard Kaulich, Diamond Light Source, for the helpful discussion.

Notes and references

^a Magnetic Resonance Center - CERM, University of Florence, Via Luigi Sacconi 6, 50019, Sesto Fiorentino, Florence, Italy

^b Department of Biomedical, Clinical and Experimental Sciences, University of Florence, Viale Morgagni 50, 50134, Florence, Italy

^c Elettra-Sincrotrone Trieste, Area Science Park, 34149, Basovizza, Trieste, Italy

^d Department of Chemistry, University of Florence, Via della Lastruccia 3, 50019, Sesto Fiorentino, Florence, Italy

† Electronic Supplementary Information (ESI) available: Supplementary Methods and Supplementary Figures S1-S4. See DOI: 10.1039/c000000x/

- (a) S. Reckel, F. Löhr, and V. Dötsch, *Chembiochem*, 2005, **6**, 1601–1606; (b) D. S. Burz, K. Dutta, D. Cowburn, and A. Shekhtman, *Nat Protoc*, 2006, **1**, 146–152; (c) P. Selenko and G. Wagner, *J. Struct. Biol.*, 2007, **158**, 244–253; (d) D. Sakakibara, A. Sasaki, T. Ikeya, J. Hamatsu, T. Hanashima, M. Mishima, M. Yoshimasu, N. Hayashi, T. Mikawa, M. Wälchli, B. O. Smith, M. Shirakawa, P. Güntert, and Y. Ito, *Nature*, 2009, **458**, 102–105; (e) C. O. Barnes, W. B. Monteith, and G. J. Pielak, *Chembiochem*, 2011, **12**, 390–391.
- (a) K. Inomata, A. Ohno, H. Tochio, S. Isogai, T. Tenno, I. Nakase, T. Takeuchi, S. Futaki, Y. Ito, H. Hiroaki, and M. Shirakawa, *Nature*, 2009, **458**, 106–109; (b) S. Ogino, S. Kubo, R. Umemoto, S. Huang, N. Nishida, and I. Shimada, *J. Am. Chem. Soc.*, 2009, **131**, 10834–10835; (c) L. Banci, L. Barbieri, E. Luchinat, and E. Secci, *Chem. Biol.*, 2013, **20**, 747–752.
- L. Banci, L. Barbieri, I. Bertini, E. Luchinat, E. Secci, Y. Zhao, and A. R. Aricescu, *Nat. Chem. Biol.*, 2013, **9**, 297–299.
- L. Yang, R. McRae, M. M. Henary, R. Patel, B. Lai, S. Vogt, and C. J. Fahrni, *Proc. Natl. Acad. Sci. U.S.A.*, 2005, **102**, 11179–11184.
- (a) T. Paunesku, S. Vogt, J. Maser, B. Lai, and G. Woloschak, *J. Cell. Biochem.*, 2006, **99**, 1489–1502; (b) R. McRae, B. Lai, S. Vogt, and C. J. Fahrni, *J. Struct. Biol.*, 2006, **155**, 22–29; (c) (d) S. Corezzi, L. Urbanelli, P. Cloetens, C. Emiliani, L. Helfen, S. Bohic, F. Elisei, and D. Fioretto, *Analytical Biochemistry*, 2009, **388**, 33–39.
- L. Y. Chang, J. W. Slot, H. J. Geuze, and J. D. Crago, *J. Cell Biol.*, 1988, **107**, 2169–2179.
- (a) V. C. Culotta, L. W. Klomp, J. Strain, R. L. Casareno, B. Krems, and J. D. Gitlin, *J. Biol. Chem.*, 1997, **272**, 23469–23472; (b) Y. Furukawa, A. S. Torres, and T. V. O'Halloran, *EMBO J.*, 2004, **23**, 2872–2881; (c) L. Banci, I. Bertini, F. Cantini, T. Kozyreva, C. Massagni, P. Palumaa, J. T. Rubino, and K. Zovo, *Proc. Natl. Acad. Sci. U.S.A.*, 2012, **109**, 13555–13560.
- C. R. Pope, C. J. De Feo, and V. M. Unger, *Proc. Natl. Acad. Sci. U.S.A.*, 2013, **110**, 20491–20496.
- A. Krezel and W. Maret, *J. Biol. Inorg. Chem.*, 2006, **11**, 1049–1062.
- S. Roudeau, A. Carmona, L. Perrin, and R. Ortega, *Anal Bioanal Chem*, 2014.
- T. Ashino, V. Sudhahar, N. Urao, J. Oshikawa, G.-F. Chen, H. Wang, Y. Huo, L. Finney, S. Vogt, R. D. McKinney, E. B. Maryon, J. H. Kaplan, M. Ushio-Fukai, and T. Fukai, *Circ. Res.*, 2010, **107**, 787–799.
- (a) G. K. Andrews, *Biochem. Pharmacol.*, 2000, **59**, 95–104; (b) L. Chen, L. Ma, Q. Bai, X. Zhu, J. Zhang, Q. Wei, D. Li, C. Gao, J. Li, Z. Zhang, C. Liu, Z. He, X. Zeng, A. Zhang, W. Qu, Z. Zhuang, W. Chen, and Y. Xiao, *J. Biol. Chem.*, 2014, **289**, 22413–22426.
- (a) R. Ortega, P. Cloetens, G. Devès, A. Carmona, and S. Bohic, *PLoS ONE*, 2007, **2**, e925; (b) L. Pascolo, A. Gianoncelli, B. Kaulich, C. Rizzardi, M. Schneider, C. Bottin, M. Polentarutti, M. Kiskinova, A. Longoni, and M. Melato, *Part Fibre Toxicol*, 2011, **8**, 7; (c) S. Vogt and M. Ralle, *Anal Bioanal Chem*, 2013, **405**, 1809–1820; (d) M. W. Bourassa, H. H. Brown, D. R. Borchelt, S. Vogt, and L. M. Miller, *Front Aging Neurosci*, 2014, **6**, 110.
- (a) K. Bertrand, S. Reverdatto, D. S. Burz, R. Zitomer, and A. Shekhtman, *J. Am. Chem. Soc.*, 2012, **134**, 12798–12806; (b) L. Barbieri, E. Luchinat, and L. Banci, *Biochim. Biophys. Acta*, 2014, **1843**, 2492–2496.